J Physiol 587.13 (2009) pp 3189–3205

Multiple forms of activity-dependent intrinsic plasticity in layer V cortical neurones *in vivo*

Jeanne T. Paz[1], Séverine Mahon[1,2], Pascale Tiret[1], Stéphane Genet[3,4,5], Bruno Delord[3,4,5] and Stéphane Charpier[1,2,5]

[1] *INSERM U 667, Collège de France, F-75005, Paris, France*
[2] *Centre de Recherche de l'Institut du Cerveau et de la Moelle épinière, UPMC/INSERM UMR-S 975; CNRS UMR 7225, Hôpital Pitié-Salpêtrière, F-75013, Paris, France*
[3] *UPMC Univ Paris 06, UMR 7222, ISIR, 4 place Jussieu, F-75005, Paris, France*
[4] *CNRS, UMR 7222, 4 place Jussieu, F-75005, Paris, France*
[5] *UPMC Univ Paris 06, F-75005, Paris, France*

Synaptic plasticity is classically considered as the neuronal substrate for learning and memory. However, activity-dependent changes in neuronal intrinsic excitability have been reported in several learning-related brain regions, suggesting that intrinsic plasticity could also participate to information storage. Compared to synaptic plasticity, there has been little exploration of the properties of induction and expression of intrinsic plasticity in an intact brain. Here, by the means of *in vivo* intracellular recordings in the rat we have examined how the intrinsic excitability of layer V motor cortex pyramidal neurones is altered following brief periods of repeated firing. Changes in membrane excitability were assessed by modifications in the discharge frequency *versus* injected current (*F–I*) curves. Most (∼64%) conditioned neurones exhibited a long-lasting intrinsic plasticity, which was expressed either by selective changes in the current threshold or in the slope of the *F–I* curve, or by concomitant changes in both parameters. These modifications in the neuronal input–output relationship led to a global increase or decrease in intrinsic excitability. Passive electrical membrane properties were unaffected by the intracellular conditioning, indicating that intrinsic plasticity resulted from modifications of voltage-gated ion channels. These results demonstrate that neocortical pyramidal neurones can express *in vivo* a bidirectional use-dependent intrinsic plasticity, modifying their sensitivity to weak inputs and/or the gain of their input–output function. These multiple forms of experience-dependent intrinsic changes, which expand the computational abilities of individual neurones, could shape new network dynamics and thus might participate in the formation of mnemonic motor engrams.

(Received 16 January 2009; accepted after revision 6 May 2009; first published online 11 May 2009)
Corresponding author S. Charpier: INSERM U667, Collège de France, 11 place Marcelin Berthelot, 75231 Paris Cedex 05, France. Email: stephane.charpier@college-de-france.fr

Memory formation in the brain is thought to result from durable experience-dependent modifications in neuronal networks. There has been much interest in activity-dependent changes in synaptic strength, which can occur at excitatory and inhibitory connections and take the form of long-term potentiation or depression (Bear, 2003; Kim & Linden, 2007). Supporting their probable implication in the establishment of memory traces, there is now conclusive evidence that changes in synaptic efficacy can be produced by behavioural training (see for review Martin & Morris, 2002). However, neurones can also modify their responsiveness to synaptic inputs through activity-dependent modification of their intrinsic excitability, due to specific changes in the function of non-synaptic ion channels. Such a modulation of cellular excitability may have a major impact on the dynamics of neuronal networks and thus could provide an additional mechanism for information storage (Marder, 1998; Golowasch *et al.* 1999).

Use-dependent plasticity of intrinsic excitability has been reported in numerous regions of the brain, including hippocampus, cerebellum and neocortex (see for reviews Daoudal & Debanne, 2003; Zhang & Linden, 2003). Neocortical pyramidal neurones can undergo diverse forms of activity-dependent intrinsic plasticity underlying

J. T. Paz and S. Mahon contributed equally to this work.
B. Delord and S. Charpier contributed equally to the supervision of the work.

DOI: 10.1113/jphysiol.2009.169334

homeostatic or mnemonic functions. A reduced synaptic drive in visual cortex cultures induces a slowly developing increase in intrinsic excitability due to a differential modulation of inward and outward voltage-gated ion channels, keeping cortical neurones within a constant operating range (Desai *et al.* 1999). Besides its role in homeostasis functions, which could be a permissive process for storage of new information, intrinsic plasticity in neocortical neurones may also provide an active mechanism for memory formation. In conscious cats, an increased excitability of motor cortical neurones, evidenced by an increase in membrane input resistance and current-evoked firing rate, is associated with the acquisition of the eye-blink reflex (Woody *et al.* 1991; Aou *et al.* 1992). More recently, it has been shown that layer V pyramidal neurones from visual cortex slices exhibit, following repeated direct stimulations, a calcium-dependent long-lasting potentiation in their intrinsic excitability manifested by a decrease in the current and voltage threshold of action potentials (Cudmore & Turrigiano, 2004). Moreover, synaptic activation of metabotropic glutamate receptors triggers a long-term increase in the membrane excitability of sensorimotor neocortical pyramidal neurones *in vitro*, leading to an enhanced probability of discharge in response to incoming synaptic inputs (Sourdet *et al.* 2003).

Although it is now well demonstrated that the intrinsic excitability of neocortical neurones can undergo activity-dependent modifications, their induction and expression properties have been poorly explored in an intact brain. Here, by the means of intracellular recordings in the rat, we have unveiled the multiple forms of intrinsic plasticity that can be encountered *in vivo* in layer V motor cortex pyramidal neurones following short periods of repeated firing and have determined their respective impact on the neuronal input–output function.

Methods

Animal preparation

Experiments were performed *in vivo* on 21 adult (2–3 months old) Sprague–Dawley rats (Charles River, L'Arbresle, France). All experiments were performed in accordance with local Ethical Committee and European Union guidelines (directive 86/609/EEC), and every precaution was taken to minimize stress and the number of animals used in each series of experiments. Animals were initially anaesthetized with sodium pentobarbital (40 mg kg^{-1}, I.P.; Sanofi, Libourne, France) and ketamine (100 mg kg^{-1}, I.P.; Imalgène, Merial, France). A cannula was inserted into the trachea and the animal was placed in a stereotaxic frame. Wounds and pressure points were repeatedly (every 2 h) infiltrated with lidocaine (lignocaine; 2%). The heart rate was monitored throughout the experiments and a surface electroencephalogram (EEG) was continuously recorded to assess the depth of anaesthesia. Additional doses of pentobarbital (10–15 mg kg^{-1}, I.P.) were regularly administered to maintain a relatively constant pattern of EEG activity. To obtain long-lasting stable intracellular recordings, rats were immobilized with gallamine triethiodide (40 mg, I.M., every 2 h; Specia, Paris, France) and artificially ventilated. Body temperature was maintained (36.5–37.5°C) with a homeothermic blanket. At the end of the experiments, animals received an overdose of sodium pentobarbital (200 mg kg^{-1}, I.P.).

Electrophysiological recordings

EEG recordings were made with low impedance (∼60 kΩ) silver electrodes placed on the dura above the primary motor cortex (12 mm anterior to the interaural line; 4–4.5 mm lateral to the midline) (Paxinos & Watson, 1986). The reference electrode was placed in a muscle at the side of the head. Intracellular recordings were obtained with glass micropipettes filled with 2 M potassium acetate (50–70 MΩ). Cortical cells were recorded in layer V of the motor cortex (see Fig. 1*A* and *B*), underneath the surface EEG electrode, at the following coordinates: 11.7–12.2 mm anterior to the interaural line, 3–4.3 mm lateral to the midline, and 1–2.8 mm under the cortical surface.

Morphological identification

Recorded neurones were labelled using an intracellular injection of 1–1.3% Neurobiotin tracer (Vector Laboratories, Burlingame, CA, USA) added to the pipette solution. Depolarizing current pulses (0.5–1 nA; 100–200 ms duration) were applied at a frequency of 1–2 Hz for a 15 min period to obtain a reliable labelling of neuronal processes (see Fig. 1*B*). The histochemical methods used to reveal the morphology of Neurobiotin-filled neurones are described in detail elsewhere (Polack & Charpier, 2006). The location of labelled neurones within the primary motor cortex was determined using the atlas of Paxinos & Watson (1986).

Data acquisition and analysis

Intracellular recordings were obtained under current-clamp conditions using the active bridge mode of an Axoclamp-2B amplifier (Molecular Devices, Union City, CA, USA). Recordings were digitized at a sampling rate of 10–20 kHz for intracellular signals and 1 kHz for EEG signals. Spectral analysis of EEG potentials was performed by applying fast Fourier transforms using Spike2 software (Cambridge Electronic Design Ltd, Cambridge, UK). Cross-correlograms between

subthreshold intracellular activity (10 s of continuous recording down-sampled at 1 kHz) and EEG waveforms, with the cortical wave as the reference signal, were calculated using Spike2. Measurements of apparent membrane input resistance and time constant were based on the linear electrical cable theory applied to an idealized isopotential neuron (Rall, 1969). Membrane input resistance was measured from the linear portion of the voltage–current (V–I) relationships or from the mean ($n \geq 10$) membrane potential change produced by hyperpolarizing current pulses of low intensity (−0.3 to −0.6 nA, 200 ms duration, applied every 1.25 s), and the membrane time constant was determined from an exponential fit to the hyperpolarization. Average membrane potential (V_m) of cortical neurones was determined from continuous recordings of at least 10 s. When necessary, membrane potential values were corrected by subtracting the extracellular tip potential measured immediately after the loss of the intracellular recording. The amplitude of action potentials was calculated as the potential difference between their voltage threshold, measured as the membrane potential at which the dV/dt exceeded $10\,V\,s^{-1}$ (Mahon *et al.* 2003), and their peak. Numerical values are given as means ± S.E.M. Statistical significances were assessed using Student's t tests, Wilcoxon signed rank test, Mann–Whitney rank sum test, one-way analysis of variance or Kruskal–Wallis one-way analysis of variance on ranks. Statistical analysis was performed with Origin 7.0 (OriginLab Corp., Northampton, MA, USA) and SigmaStat 3.1 (SPSS Inc., Chicago, IL, USA).

Assessment of intrinsic excitability and conditioning procedures

Intrinsic excitability was assessed, in control and post-conditioning periods, by measuring the firing rate evoked by a range of depolarizing square current pulses (200–500 ms; 0.2–1.8 nA), and also basic electrophysiological properties, including the cell input resistance, membrane time constant and the value of the membrane potential at the onset of current pulses (Fig. 2*A* and *C*). Since the current-evoked firing could exhibit a trial-to-trial variability due to collisions with the background synaptic activity inherent in *in vivo* preparations, current pulses of a given intensity were applied 10–20 times every 1.25–10 s and the corresponding firing rates were averaged. The mean firing frequency *versus* the intensity of injected current (F–I) curves were constructed accordingly. Two parameters were then extracted from the linear fits of these neuronal input–output relationships (see below for details), i.e. the current threshold (θ, the minimal current intensity necessary for the generation of an action potential) and the slope of the F–I curve (γ). An extrapolated value of θ was obtained from the F–I curve, as the intersection of the corresponding linear fit with the axis of current intensities.

Conditioning protocols (Fig. 2*B*) consisted of repeated injections of suprathreshold current (0.3–1.8 nA) pulses (103.8 ± 5.1 pulses; range, 53–182; $n = 33$ cells) of 500 ms duration applied every 5 s. This protocol of stimulation generated a mean evoked firing rate of 32.5 ± 2.6 Hz (range, 11–63 Hz; $n = 33$ cells), leading to a total number of evoked action potentials (including the spontaneous discharge between current pulses; see Fig. 2*B*) of 2 472.4 ± 280.6 ($n = 33$). The pattern of activity in cortical cells during the induction protocols was similar to the discharge of motor cortex neurones (5–60 Hz) associated with associative behavioural learning (see Birt *et al.* 2003).

Linear fits and statistical analysis of activity-dependent changes in *F–I* curves

The threshold and the slope of the F–I curves were estimated as follows. The Model I linear regressions of the F–I relationships were computed for each neuron in control and post-conditioning conditions. These relationships were expressed as $F = \gamma_X(I - \theta_X)$, where X denotes the condition (i.e. control or post-conditioning), $\gamma_X = \mathrm{cov}_X(I, F)/\sigma^2_{IX}$ is the slope (Hz nA^{-1}), $\theta_X = m_{IX} - m_{FX}\sigma^2_{IX}/\mathrm{cov}_X(I, F)$ is the current threshold (nA) and m_{IX}, m_{FX}, σ^2_{IX} and $\mathrm{cov}_X(I, F)$, respectively denote the means of I and F, the variance of I and the covariance between I and F. The statistical significance of the regression was assessed with the test of the correlation coefficient, i.e. a t test with statistic $t_{rX} = r_X\sqrt{n_X - 2}/\sqrt{1 - r^2_X}$ and $n_X - 2$ degrees of freedom (r_X is the coefficient of regression and n_X the number of observations). Neurones with significant correlation ($P < 0.05$) in both conditions were further analysed to investigate modifications in the threshold and/or in the slope of the F–I curve after conditioning.

A modification of γ after conditioning was statistically assessed in each neurone by a t test with statistic $t_\gamma = |\gamma_{Post} - \gamma_{Cont}|/\sigma_{d\gamma}$ and $n_{Cont} + n_{Post} - 4$ degrees of freedom, at the level 0.05. Here, $\sigma_{d\gamma}$ denotes the standard deviation of the difference between slopes ($\sigma^2_{d\gamma} = \sigma^2_{\gamma Cont} + \sigma^2_{\gamma Post}$). The standard deviation of the slope for each condition was computed as

$$\sigma^2_{\gamma X} = (n_X - 1)^{-1}\sigma^2_{FI}\sigma^{-2}_{IX},$$

where

$$\sigma^2_{FI} = (n_{Cont} + n_{Post} - 4)^{-1}\big((n_{Cont} - 2)\sigma^2_{FICont} + (n_{Post} - 2)\sigma^2_{FIPost}\big)$$

denotes the weighted unexplained variance of the F–I linear regression, with

$$\sigma^2_{FIX} = (n_X - 2)^{-1}\sum_{k=1}^{n_X}(F_k - \gamma_X(I_k - \theta_X))^2$$

being the unexplained variance in the X condition (Sokal & Rohlf, 1995).

A direct test assessing threshold differences between control and post-conditioning conditions is not feasible because it is impossible to estimate the standard deviation of the x-intercept of a linear regression curve (Sokal & Rohlf, 1995). However, the y-intercept of the opposite I–F linear regression constitutes an estimate of the current threshold for spiking that can be assessed statistically. We thus computed the (Model I) linear regression of the I–F relation for each neurone in both conditions, which was expressed as $I = \theta'_X + F/\gamma'_X$. Here, θ'_X (nA) is the current threshold (i.e. the y-intercept) of the I–F regression. A modification of the threshold during the conditioning was statistically assessed in each neurone by a t test with statistic $t_{\theta'} = |\theta'_{Post} - \theta'_{Cont}|/\sigma_{d\theta'}$ and $n_{Cont} + n_{Post} - 4$ degrees of freedom, at the level 0.05. Here, $\sigma_{d\theta'} = \sqrt{\sigma^2_{\theta' Cond} + \sigma^2_{\theta' Post}}$ represents the standard deviation of the difference between thresholds, where $\sigma^2_{\theta' Cont}$ and $\sigma^2_{\theta' Post}$ denote the threshold variance in each condition. These variances are expressed as

$$\sigma^2_{\theta' X} = \sigma^2_{IF}\left(n_X^{-1} + (n_X - 1)^{-1} m^2_{FX} \sigma^{-2}_{FX}\right),$$

where

$$\sigma^2_{IF} = (n_{Cont} + n_{Post} - 4)^{-1}\left((n_C - 2)\sigma^2_{IFCont} + (n_T - 2)\sigma^2_{IFPost}\right)$$

is the weighted unexplained variance of the I–F linear regression, with

$$\sigma^2_{IFX} = (n_X - 2)^{-1} \sum_{k=1}^{n_X} (I_k - (\theta'_X + F_k/\gamma'_X))^2.$$

Results

Morphological and electrophysiological characterization of recorded neurones

We made *in vivo* intracellular recordings from cortical neurones ($n = 43$ cells) located in the primary motor cortex simultaneously with the corresponding surface EEG. The depth of intracellular records, between 1039 and 2816 μm from the cortical surface (1803 $\pm$ 70 μm, $n = 43$), suggested that the recorded neurones were exclusively located in layer V (Fig. 1*A*). This was confirmed by subsequent histological analysis of intracellularly labelled cells ($n = 7$), which exhibited the typical morphological features of cortical pyramidal neurones (Feldman, 1984), including a rhomboidal cell body, a prominent apical dendrite extending vertically towards the pial surface and basal dendrites radiating out from the base of the soma (Fig. 1*B*). Injection of positive current pulses showed that most cells (39 out of 43) exhibited the typical firing pattern of regular spiking (RS) neocortical neurones, with variable rates of adaptation (see Figs 1*Ca*, 2*A*, 4*A*, 6*A* and 8*A*), whereas the remaining neurones ($n = 4$) displayed a firing profile characteristic of intrinsic bursting (IB) cells (see Figs 1*Cb* and 5*A*) (Connors & Gutnick, 1990; Steriade, 2004).

The passive electrical membrane properties of recorded cortical neurones, as measured in control periods, were similar to those previously described from motor cortex neurones in cats (Baranyi *et al.* 1993) or rats (Mahon *et al.* 2001; Paz *et al.* 2005; Polack & Charpier, 2006). Cortical cells displayed a membrane potential of -65.2 ± 0.4 mV (from -70.6 to -58.0 mV, $n = 43$) (Fig. 1*Ec*), an apparent input resistance, which could be measured from the linear portion of the V–I curve (Fig. 1*D*), of 21.6 ± 0.9 MΩ (from 11.9 to 33 MΩ, $n = 43$) and a membrane time constant (Fig. 1*D*, inset) ranging between 4.6 and 15.9 ms (8.9 ± 0.4 ms, $n = 43$). Action potentials had an amplitude ranging from 50.0 to 80.7 mV (65.0 ± 1.2 mV, $n = 43$), a total duration of 1.59 ± 0.07 ms and a voltage threshold of -51.7 ± 0.4 mV (from -55.0 to -45.0 mV).

Assessment of neuronal excitability

The intrinsic excitability in response to depolarizing current pulses was quantified by the slope (γ) of the F–I curves, which is an index of the gain of neuronal input–output function, and the threshold current intensity (θ) (Fig. 1*D*). The values of γ, measured from the linear fits of the F–I curves (Fig. 1*D*) (see Methods), displayed a high cell-to-cell variability, from 14.8 to 84.5 Hz nA^{-1} with a mean of 49.4 ± 2.7 Hz nA^{-1} ($n = 38$ cells). Because most recorded cortical neurones were spontaneously active (40 out of 43), it was difficult to determine experimentally the minimum current intensity just able to generate a single action potential. However, an extrapolation of θ could be obtained from the linear fits of the F–I curves (Fig. 1*D*) (see Methods). Across cells, the mean value of θ was 0.20 ± 0.04 nA ($n = 38$) in accordance with that previously calculated from the same cortical region (Baranyi *et al.* 1993; Paz *et al.* 2005).

The background intracellular activity of cortical neurones was characterized by oscillating voltage fluctuations (Figs 1*Ea*, 6*Ca* and 7*C*), probably due to ongoing synaptic inputs, which generated a low firing rate (1.6 ± 0.4 Hz, $n = 40$ cells; Figs 1*Ea* and 7*C*) or remained subthreshold for action potential discharge ($n = 3$ cells; Fig. 6*Ca*). The rhythmic spontaneous membrane potential variations in the recorded neurones were consistently correlated with the corresponding EEG waves (Fig. 1*Ea*, inset), which provide a reliable reflection of coherent synaptic activities in the related cortical networks (Creutzfeld *et al.* 1966; Mahon *et al.* 2001).

Stability of intrinsic excitability during control stimuli

We first ascertained the stability of neuronal intrinsic excitability during the repeated application of control current pulses. In seven RS neurones, we applied 2–4 successive (every 10–30 min) series of constant-amplitude positive current pulses, using a single ($n = 2$ cells; Fig. 3*A*) or multiple ($n = 5$ cells; Fig. 1 in Supplemental material, available online only) inter-stimulus intervals (ISIs), which ranged from 1.25 to 10 s. In the control experiment illustrated in Fig. 3*A*, using an ISI of 2.25 s, despite a

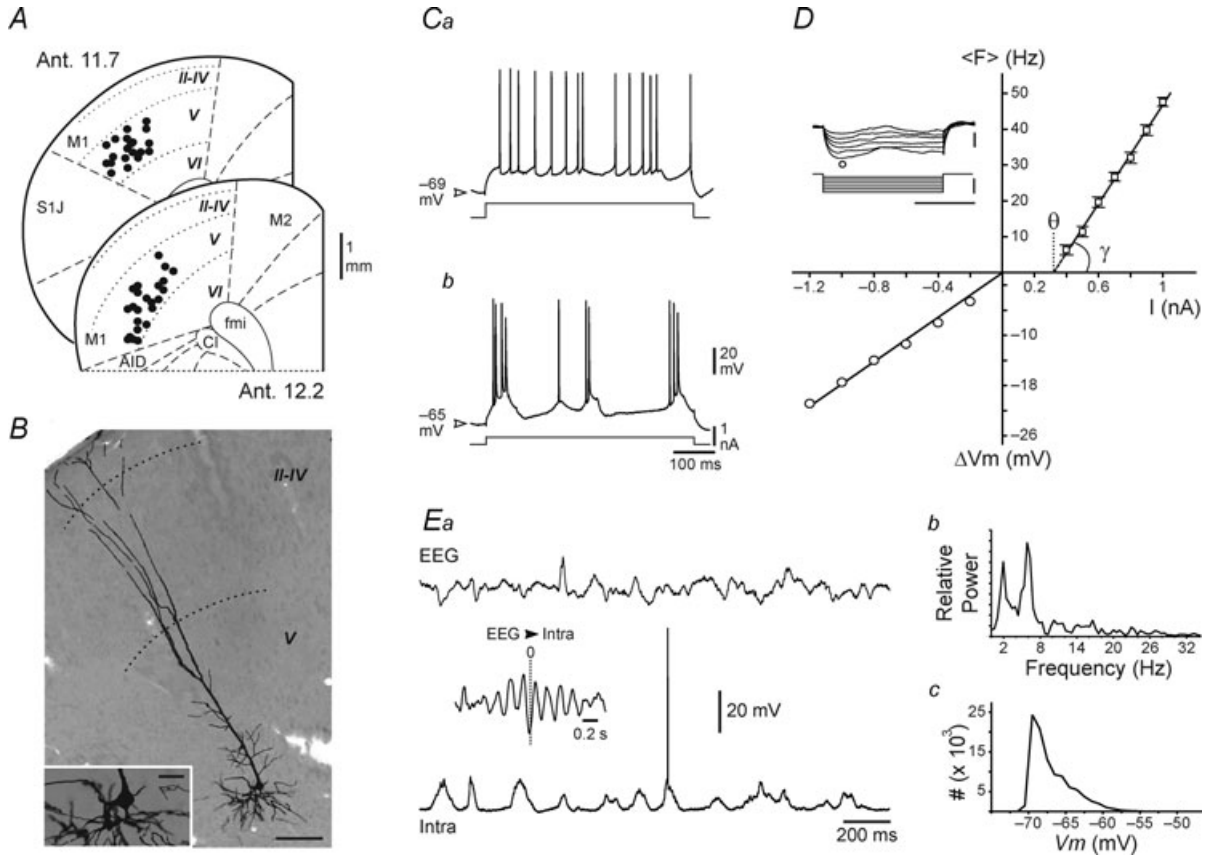

Figure 1. Morphological and electrophysiological properties of recorded cortical neurones
A, superimposed brain slice drawings, at the indicated distances (in millimetres) from the lambda (adapted from Paxinos & Watson, 1986), showing the location of intracellular recordings within layer V of the primary motor cortex (M1). AID, agranular insular cortex, dorsal part; Cl, claustrum; fmi, forceps minor of the corpus callosum; M2, secondary motor cortex; S1J, primary somatosensory cortex, jaw region. *B*, microphotographs of a Neurobiotin-injected cortical pyramidal neurone whose soma was located in the layer V of M1. Calibration: 200 μm. The enlarged view of the somatodendritic region (calibration: 50 μm) clearly shows the typical morphological features of pyramidal neocortical neurones. *C*, intracellular responses (top records) to 500 ms suprathreshold current pulses (bottom traces) from a regular spiking (RS) (*Ca*) and an intrinsic bursting (IB) (*Cb*) neurone. Calibrations in *Cb* apply also to *Ca*. *D*, plots of averaged voltage changes (ΔV, open circles) and mean firing frequency (<*F*>, open squares) as a function of current intensities. The membrane input resistance (20 MΩ) was measured from the ohmic portion of the *V*–*I* curve (linear fit; $r^2 = 0.99$, $P < 0.0001$). The *F*–*I* relationship, which was linear in the range of applied currents ($r^2 = 0.99$; $P < 0.0001$), allowed the extraction of two parameters of intrinsic excitability, the slope (γ) of the input–output relationship and the current threshold (θ), which was approximated following graphic extrapolation. Each data point in the *F*–*I* plot represents the mean (± S.E.M) firing rate measured from 20 successive trials. The inset depicts the mean ($n > 12$ trials) current-evoked (bottom traces) voltage drops (top traces) used to construct the corresponding *V*–*I* curve. The membrane potential changes were measured at the time indicated by the open circle. Calibrations: 100 ms, 1 nA, 10 mV. *Ea*, continuous (2 s) intracellular recording (Intra) from the RS neuron shown in *B* and the corresponding surface EEG activity (top trace). The inset depicts the cross-correlation between the EEG and intracellular activities (10 s of continuous activity), using the cortical surface activity as reference. Note the high correlation between the two oscillatory signals at a frequency of 5.7 Hz. *Eb* and *c*, corresponding EEG relative power spectrum (*b*) and membrane potential (V_m) distribution (*c*; bin, 1 mV) computed from continuous records of at least 10 s. Panels *B*, *Ca*, *D* and *E* are from the same neurone.

trial-to-trial variability (top traces), the average firing frequency (Control 1, $<F> = 15.7 \pm 0.7$ Hz; Control 2, $<F> = 14.5 \pm 0.7$ Hz; Control 3, $<F> = 15.7 \pm 0.8$ Hz; $P > 0.4$; Fig. 3*A*, dashed lines in the top graph) and the mean pre-pulse membrane potential (Control 1, $V_m = -63.8 \pm 0.9$ mV; Control 2, $V_m = -65.1 \pm 1.0$ mV; Control 3, $V_m = -64.7 \pm 0.8$ mV; $P > 0.35$; Fig. 3*A*, bottom graph) remained stable throughout the control session. In neurones where different control protocols were tested, we found that the successive application of series of 10–20 current pulses, with ISIs of 1.25 s, 2.25 s and 10 s, did not affect the neuronal excitability, as attested by the stability of the evoked firing rate (Supplemental Fig. 1). Furthermore, we did not detect any significant changes in the membrane input resistance and time constant when measured between the series of current pulses (not shown). The specific effectiveness of the conditioning procedures (see Methods) for inducing intrinsic plasticity was demonstrated by the relative constancy of evoked neuronal spiking during successive control sets of stimulations, with three different ISIs, whereas the continuous application of an elevated number of current pulses ($n > 100$) led to a robust increase in cell responsiveness (Supplemental Fig. 1*B*).

The constancy of *F–I* curve parameters was further demonstrated in six neurones (5 RS and 1 IB) where two complete sets of control stimulations were applied successively (every 10–30 min) (Fig. 3*B*). These cells displayed electrophysiological properties in the middle range of values calculated from the overall neuronal population ($V_m = -65.3 \pm 1.6$ mV, input resistance $= 23.7 \pm 2.4$ MΩ, spontaneous firing rate $= 1.1 \pm 0.7$ Hz; $n = 6$ cells). As illustrated in Fig. 3*B*, the parameters of the *F–I* relationship remained stable within each cell ($P > 0.13$ for both γ and θ) throughout the control stimulation periods. The mean values of γ and θ were also found unchanged between the first and second control *F–I* curves (Control 1, $\gamma = 45.4 \pm 8.4$ Hz nA^{-1}; $\theta = 0.21 \pm 0.10$ nA; Control 2, $\gamma = 42.8 \pm 7.1$ Hz nA^{-1}; $\theta = 0.22 \pm 0.08$ nA, $n = 6$ cells; $P > 0.25$ for each parameter; Fig. 3*Bb*, inset). This lack of change in membrane responsiveness was not due to an inability of these neurones to modify their intrinsic excitability since three of these control cells could be potentiated or depressed when a subsequent conditioning protocol was applied (see Supplemental Fig. 1*B*).

Intrinsic plasticity expressed as a leftward shift in the *F–I* curve

In four cells, the intracellular conditioning induced a significant increase in intrinsic excitability expressed as a leftward shift in the *F–I* curve, i.e. a decrease in θ values, without any significant modification in the corresponding slope (Fig. 4). This subset of cells ($n = 4$) displayed, during baseline periods, a mean membrane potential of -64.6 ± 0.9 mV, an input resistance of 15.0 ± 1.2 MΩ, a membrane time constant of 7.9 ± 1.2 ms and a voltage firing threshold of -48.9 ± 1.1 mV. One cell was silent at rest and the average spontaneous firing frequency in the three active neurones was 0.55 ± 0.33 Hz. The intracellular conditioning consisted of repeated injections of current pulses (0.4–1.8 nA, $n = 79$–120 pulses, $n = 4$ cells) leading to a mean evoked firing rate of 27.2 ± 10.2 Hz. As exemplified by the RS neuron shown in Fig. 4,

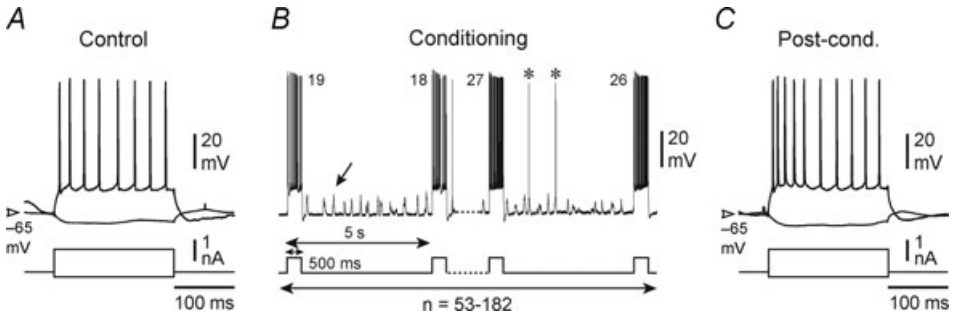

Figure 2. Assessment of intrinsic excitability and conditioning protocols
A and *C*, intrinsic excitability of cortical neurones was assessed in control (*A*) and after conditioning (*C*) by the measurement of voltage changes in response to negative current pulses and mean firing rates evoked by positive current pulses. Control and post-conditioning *V–I* and *F–I* curves were then constructed using all tested current pulses (see Fig. 1*D*). Here, and in the following figures, the membrane potential values are indicated at the left of the intracellular records. *B*, conditioning protocols consisted of repeated ($n = 53$–182; every 5 s) injections of 500 ms suprathreshold current pulses (bottom trace). Note the occurrence of spontaneous synaptic depolarizations (arrow) and action potentials (asterisks) between the conditioning stimuli (top trace). The 2 first and last conditioning responses are shown. In the illustrated experiment (same cell as in Fig. 8), the induction protocol resulted in an increased firing rate (*A versus C*), which was already apparent at the end of conditioning (the number of evoked action potentials is indicated next to the conditioning responses).

the conditioning protocol induced an increase in the evoked firing over the whole tested range of current intensities. This increase in membrane responsiveness was accompanied by a significant decrease of the θ value in each tested cell (θ control $= 0.48 \pm 0.18$ nA; θ post-conditioning $= 0.32 \pm 0.14$ nA, $n = 4$; $P < 0.01$) (Fig. 4*B*), corresponding to a mean reduction of $35.9 \pm 7.8\%$. The activity-dependent decrease of θ could be obtained in two RS and two IB (Fig. 5) neurones, demonstrating that this form of intrinsic plasticity was not cell-type specific. There was no concomitant change in the slope of the *F–I* curve (γ control $= 43.8 \pm 8.7$ Hz nA^{-1}; γ post-conditioning $= 44.5 \pm 7.9$ Hz nA^{-1}, $n = 4$; $P > 0.2$) (Figs 4*B* and 5*B*), suggesting that the increase in excitability resulted from a simple shift of the *F–I* curve to the left. The time course of this potentiation was assessed in three cells by monitoring the change in firing rate in response to a current pulse of constant amplitude at different times after conditioning. As shown in Fig. 4*C*, the increase in current-evoked firing persisted until the loss of intracellular recordings, up to 30 min after induction. In the three tested cells, the mean firing frequency reached $287.8 \pm 102.8\%$ of control values 25–30 min after conditioning.

We compared additional parameters of intrinsic excitability before and after the induction protocol

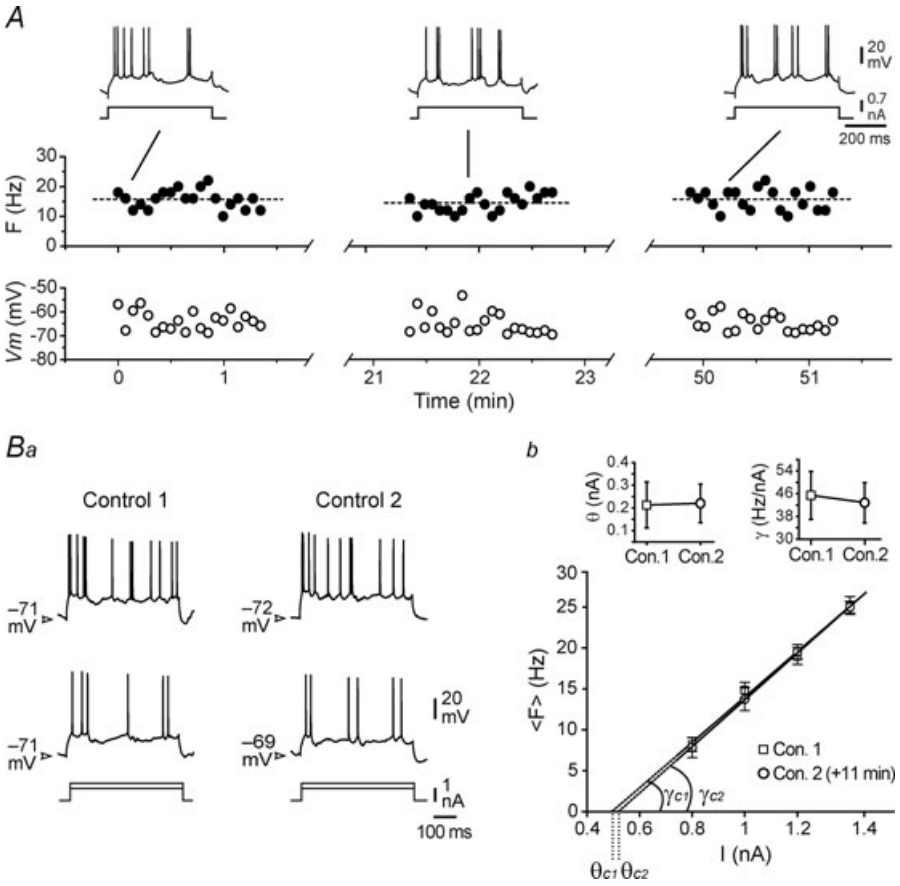

Figure 3. Stability of intrinsic excitability during control stimulations
A, time course of intracellular responses of a layer V cortical neurone to three series of control stimulations, which consisted of the injection of 20 successive (every 2.25 s) current pulses of +0.7 nA. The firing frequency (filled circles) as well as the membrane potential measured just prior to current pulses (open circles) remained stable throughout the control period. The dashed lines indicate the mean firing frequency for each series of stimulations. Examples of firing evoked in the recorded neurone at the indicated times are shown above the graph. *B*, stability of control *F–I* curve parameters. *Ba*, firing of a cortical neuron (top traces) induced by intracellular injection of +1 and +1.4 nA current pulses (bottom traces), during a first (Control 1) and a second (Control 2, +11 min) set of control stimulations, using 4 different current intensities. *Bb*, corresponding *F–I* curves. Neuronal intrinsic excitability was not modified as attested by the stability of both γ (Control 1, $\gamma_{c1} = 27.6$ Hz nA^{-1}; Control 2, $\gamma_{c2} = 28.6$ Hz nA^{-1}; $P = 0.7$) and θ (Control 1, $\theta_{c1} = 0.49$ nA; Control 2, $\theta_{c2} = 0.52$ nA; $P = 0.8$) values. The inset shows the pooled values ($n = 6$ cells) of θ and γ during the first (Con. 1) and the second (Con. 2) series of control stimulations. Each data point in the *F–I* curves represents the mean (± S.E.M) firing rate measured from 12 successive trials. *A* and *B* are from different cells.

in order to reveal possible concurrent alterations in passive membrane properties. The post-conditioning values of membrane potential (-64.2 ± 1.5 mV) (Figs 4*A* and 5*A*), input resistance (16.0 ± 2.3 MΩ) and membrane time constant (8.7 ± 1.9 ms) (Fig. 4*A*, inset) were not significantly modified ($P > 0.3$ for each parameter; $n = 4$ cells) compared to control measurements. Consistent with the decrease in the current threshold, we found a slight hyperpolarizing shift in the voltage threshold for action potential discharge after conditioning (-50.4 ± 1.3 mV, $n = 4$ cells), which was, however, not statistically significant ($P > 0.2$). Despite the reduction in the current and voltage threshold, we did not find any significant change in the mean spontaneous firing rate during the post-conditioning epoch (0.52 ± 0.24 Hz, $n = 4$ cells; $P = 0.7$) and EEG activity did not show any apparent modification (not shown).

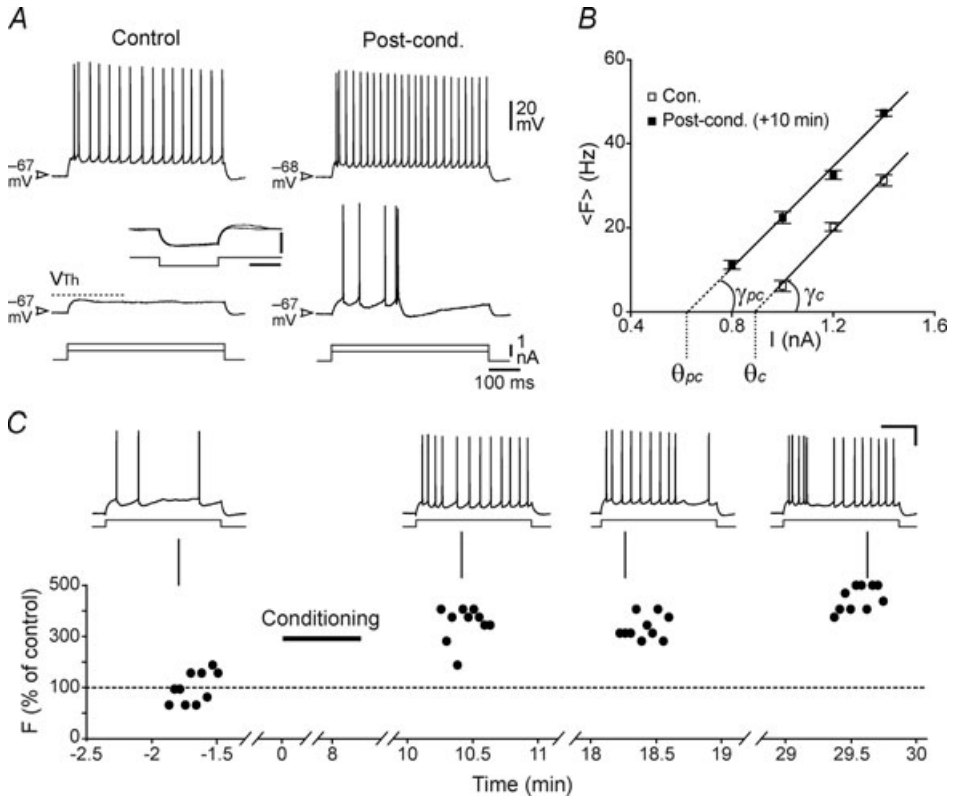

Figure 4. Activity-dependent increase in cortical neurone intrinsic excitability: leftward shift in the *F–I* curve

A, voltage responses of a RS cortical neurone (top traces) to depolarizing current pulses of increasing intensity (lower traces), in control and 10 min after intracellular conditioning (Post-cond.), which consisted of the repeated application of 500 ms current pulses ($n = 104$) of 1 nA generating a mean firing of 29 Hz. The +0.8 nA current pulse, which induced a membrane depolarization that remained below the voltage threshold for action potential discharge (VTh, dashed line) in control, could generate 5 action potentials after conditioning. A robust increase in the evoked firing rate was observed for suprathreshold current intensities whereas the membrane potential remained constant (arrowheads). The inset shows the superimposition of the mean ($n \geq 12$) voltage drops (top traces) in response to −0.6 nA current pulses (bottom traces), applied in control and after the induction of intrinsic plasticity. Note the stability of both membrane input resistance and time constant. Calibrations: 50 ms, 5 mV. *B,* corresponding *F–I* curves (linear fits, $r^2 > 0.88$; $P \leq 0.001$) obtained in control (Con.) and 10 min after conditioning. Each data point represents the mean (± S.E.M) firing rate calculated from 10 successive trials. The value of θ was significantly reduced after conditioning (θ_{pc}) (Control, $\theta_c = 0.89$ nA; Post-conditioning, $\theta_{pc} = 0.62$ nA; $P < 0.001$), whereas the corresponding slope of the *F–I* curve remained unaffected (Control, $\gamma_c = 62.5$ Hz nA^{-1}; Post-conditioning, $\gamma_{pc} = 59.1$ Hz nA^{-1}; $P > 0.4$). *C*, time course of the firing frequency change induced by the intracellular conditioning. Three series of direct stimulations (+1 nA, 500 ms, $n = 10$) were successively applied after the conditioning protocol. Changes are normalized to the mean control value (dashed line). Top, examples of the cell response to a +1 nA current pulse recorded at the indicated times. Calibrations: 150 ms, 20 mV. Results depicted in *A–C* are from the same cell.

Intrinsic plasticity expressed as an increase in the slope of the *F–I* curve

The induction protocol resulted in five cortical cells (4 RS and 1 IB) in a long-lasting (up to 40 min) enhancement of membrane excitability evidenced by an increase in the slope of the *F–I* curve, which was not associated with a significant change in the current threshold (Fig. 6*A* and *B*). The corresponding protocol of conditioning consisted of repeated ($n = 100$–182) injections of current pulses (0.4–1.8 nA), leading to a mean firing rate of 29.6 ± 6.8 Hz ($n = 5$ cells). During the baseline periods, the basic electrophysiological features of these potentiated neurones ($n = 5$) were as follows, a mean membrane potential of -65.6 ± 1.7 mV (Fig. 6*Ca*, bottom trace and *Da*, left), an input resistance of 17.2 ± 1.3 MΩ, a membrane time constant of 8.4 ± 0.9 ms and a voltage firing threshold of -50.1 ± 1.0 mV. Four cells were spontaneously active (1.8 ± 0.9 Hz) and one neurone remained silent throughout the control period. Control *F–I* curves indicated a γ of 37.4 ± 10.7 Hz nA^{-1} (range, 14.8–71.9 Hz nA^{-1}, $n = 5$) and a mean θ of 0.14 ± 0.11 nA ($n = 5$) (Fig. 6*B*). Whereas the threshold current remained unchanged after conditioning ($P > 0.5$ for each cell), γ was markedly augmented (γ post-conditioning $= 52.9 \pm 8.5$ Hz nA^{-1}, $n = 5$ cells; $P < 0.05$ for each cell), corresponding to a mean increase of 67.0 ± 38.8% (range, 14.3–197.5%) (Fig. 6*B*). Again, we did not find any significant difference between the post-conditioning values of membrane potential (-64.6 ± 1.5 mV, $n = 5$ cells; Fig. 6*Cb*, bottom trace and *Db*, left), input resistance (19.3 ± 3.0 MΩ, $n = 4$ cells), time constant (8.6 ± 1.8 ms, $n = 4$ cells), action potential voltage threshold (-50.5 ± 0.6 mV, $n = 5$ cells) and those measured during the control periods ($P > 0.1$ for each parameter). Spontaneous firing rate remained stable (post-conditioning, 2.0 ± 0.9 Hz, $n = 4$; $P = 0.1$). Moreover, spontaneous subthreshold membrane potential fluctuations (Fig. 6*D*, left), as well as corresponding pattern of EEG waves (Fig. 6*D*, right), were not modified. Accordingly, the correlated oscillatory activity between the simultaneous recorded neurone and corresponding EEG was unaffected (Fig. 6*Db*, inset), indicating that the synchronized synaptic activities within the local cortical network remained stable throughout the recording session.

Intrinsic plasticity expressed as a rightward shift in the *F–I* curve

In the experience-dependent cellular changes described above, the increase in the slope or the leftward shift of the *F–I* curve led to a global increase in intrinsic excitability. In five RS neurons, induction protocols (80–120 current pulses of 0.5–1 nA; firing rate ranged from 15 to 40 Hz) could result in a decrease in cell responsiveness, which was expressed by an increase in the current threshold correlated with a rightward shift of the complete *F–I* curve (Fig. 7*A* and *B*). As illustrated in Fig. 7*A* and *B*, this decrease in cell responsiveness was evident over the whole range of tested currents and persisted throughout the post-conditioning period (74.8 ± 5.7% of the control 20–25 min after induction, $n = 4$ cells). During control stimulations, the mean values of γ and θ were 57.3 ± 5.7 Hz nA^{-1} and 0.17 ± 0.04 nA ($n = 5$ cells), respectively. Induction of intrinsic plasticity was correlated with a robust (71.5 ± 19.3%) increase in current threshold values (θ post-conditioning $= 0.28 \pm 0.06$ nA, $n = 5$; $P < 0.025$ in each cell) (Fig. 7*B*). The control basic electrophysiological properties of these depressed neurones ($V_m = -64.7 \pm 1.5$ mV; input resistance $= 26.7 \pm 2.7$ MΩ; membrane time constant $= 10.3 \pm 1.1$ ms; action potential voltage threshold $= -47.1 \pm 2.4$ mV, $n = 5$) were not significantly affected by the induction protocol ($P > 0.2$ for each parameter) (Fig. 7*C*). In four cells, the control spontaneous firing (range, 0.3–1.6 Hz) was unaltered by the conditioning ($P > 0.35$) (Fig. 7*C*) while the remaining neurone, which exhibited an intermittent background discharge (every ~2 s), became silent after conditioning. As observed during potentiation of intrinsic excitability (see Fig. 6*Db*, inset), the coherent oscillations between depressed neurones and EEG waves were maintained (Fig. 7*C*, right).

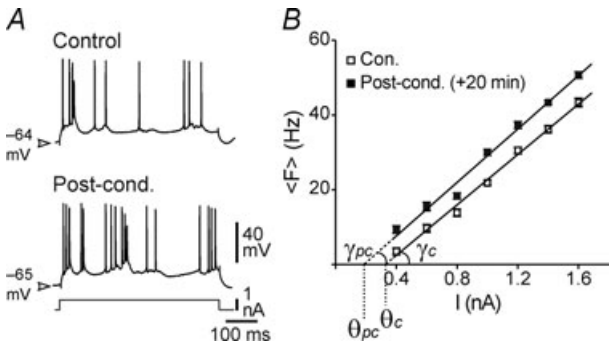

Figure 5. Leftward shift in the *F–I* curve following intracellular conditioning in an intrinsic bursting neurone
A, examples of the cell response to a +1 nA current pulse in control and 20 min after induction of intrinsic plasticity (Post-cond.). *B*, *F–I* curves (linear fits, $r^2 > 0.9$; $P < 0.001$) obtained in control (Con.) and 20 min after conditioning (+1.8 nA current pulses of 500 ms applied 80 times leading to a mean evoked firing rate of 51 Hz) show a clear-cut leftward shift. This was associated with a significant reduction of θ (Control, $\theta_c = 0.33$ nA; +20 min, $\theta_{pc} = 0.17$ nA; $P < 0.001$) and a stability in the corresponding curve slope (Control, $\gamma_c = 33.5$ Hz nA^{-1}; +20 min, $\gamma_{pc} = 35.2$ Hz nA^{-1}; $P = 0.2$). Each data point represents the mean (± S.E.M.) firing rate calculated from 12 successive trials.

Mixed changes in membrane excitability

In the different subset of neurones described above, the intrinsic plasticity, which resulted in an increase or a decrease in global cell excitability, was expressed by a modification in the slope or a sliding of the *F–I* relationship. In six cells, the intrinsic plasticity was mixed in the sense that both the current threshold and the slope of the *F–I* curve were concomitantly modified.

A decrease in θ associated with an increase in γ led in three RS neurones to a 'coherent' mixed plasticity, resulting in a global increase in membrane excitability (Fig. 8). The intracellular conditioning (80–125 current pulses of 0.6–1.1 nA; conditioning firing rate ranged from 11 to 40 Hz) induced a reduction in θ (θ control $= 0.31 \pm 0.20$ nA; θ post-conditioning $= 0.21 \pm 0.20$ nA, $n = 3$ cells;

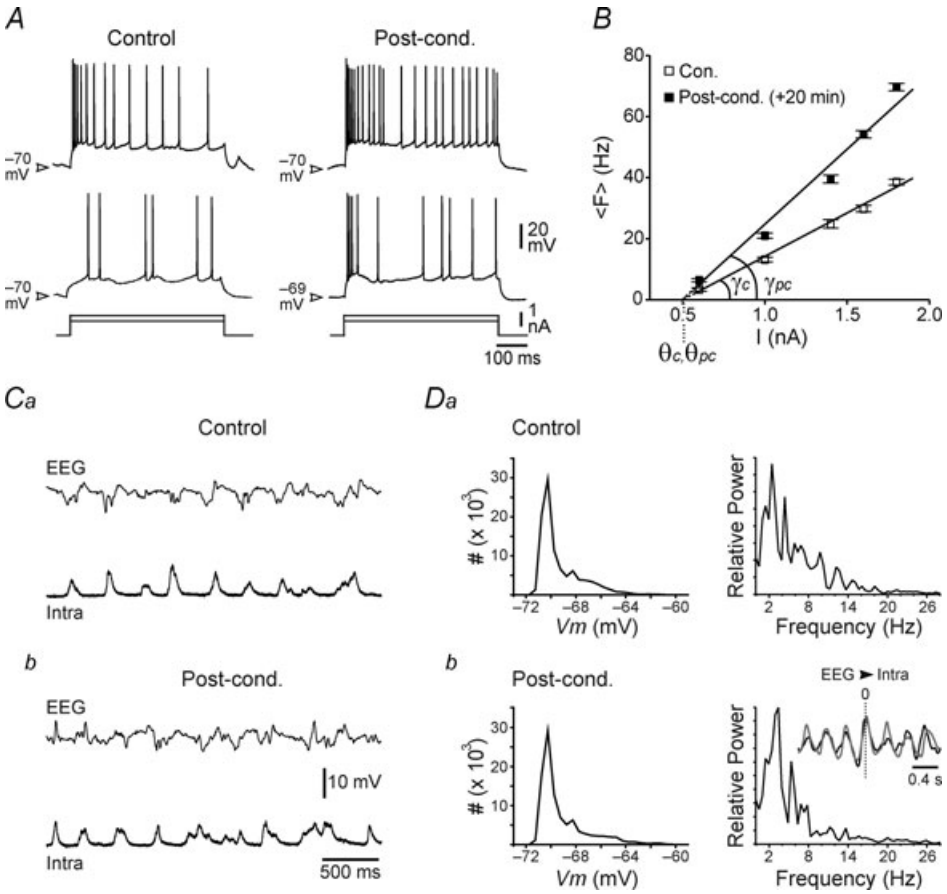

Figure 6. Activity-dependent increase in cortical neurone intrinsic excitability: increase in the slope of the *F–I* curve

A, responses of a RS neurone (top traces) to depolarizing current pulses of increasing intensity (lower traces), in control and 20 min after the induction protocol (Post-cond.). The intracellular conditioning was composed of 180 current pulses (500 ms duration) of +1.8 nA applied every 5 s, generating a mean evoked firing of 39 Hz. Note the robust increase, after conditioning, in the firing rate evoked by the different current intensities, whereas the membrane potential (arrowheads) was nearly unchanged. *B,* corresponding *F–I* curves (linear fits, $r^2 > 0.9$; $P < 0.001$) in control (Con.) and 20 min after the induction protocol. The post-conditioning value of γ was significantly augmented compared to its control value (Control, $\gamma_c = 28.8$ Hz nA^{-1}; Post-conditioning, $\gamma_{pc} = 51.8$ Hz nA^{-1}; $P < 0.001$), whereas the corresponding θ was unchanged (Control, $\theta_c = 0.52$ nA; Post-conditioning, $\theta_{pc} = 0.54$ nA; $P = 0.9$). Each data point in the *F–I* plot represents the mean (± S.E.M.) firing rate measured from 10–12 successive trials. *C,* epochs of spontaneous intracellular activity (Intra, bottom records) and corresponding EEG waves (top records), in control (*a*) and after plasticity induction (*b*). Calibrations in (*b*) apply to (*a*). *D*, corresponding membrane potential (V_m) distributions (left; bin 1 mV) and EEG power spectra (right) computed from continuous recordings of 10 s in control (*a*) and 20 min after the conditioning protocol (*b*). Note the stability of neuronal and global synaptic activities throughout the recording session. Moreover, as demonstrated by the inset (*b*, right) showing the superimposition of cross-correlograms between EEG and intracellular activities, before (black) and 22 min after (grey) conditioning, the induction of intrinsic plasticity did not alter the correlated oscillation (3.1 Hz) between both signals. All panels are from the same cell.

$P \leq 0.01$ for each cell) concomitant with an augmentation of γ (γ control $= 62.0 \pm 15.2$ Hz nA^{-1}; γ post-conditioning $= 75.1 \pm 18.6$ Hz nA^{-1}, $n = 3$ cells; $P \leq 0.02$ for each cell) (Fig. 8*B*, inset). These mixed cellular changes, which could be observed until 44 min after the induction protocol, were not correlated with a modification in baseline values of membrane potential (-66.3 ± 0.6 mV, $n = 3$), input resistance (19.8 ± 2.0 MΩ, $n = 3$), membrane time constant (7.3 ± 1.8 ms, $n = 3$) and action potential voltage threshold (-50.3 ± 1.9 mV, $n = 3$), which remained unchanged after conditioning ($P > 0.3$ for each parameter). Again, the spontaneous activity in the two active cells, as well as in the silent neurone, was not affected during plasticity expression.

Three RS neurones (Control, $V_m = -62.8 \pm 0.2$ mV; input resistance $= 22.4 \pm 5.1$ MΩ; time constant $= 8.8 \pm 0.5$ ms) experienced activity-dependent (Conditioning, 70–180 current pulses of 0.7–1.4 nA; conditioning firing rate ranged from 39 to 63 Hz) changes (lasting from 20 to 30 min) in their excitability that were apparently discordant since the *F–I* curves displayed concurrently an enhanced slope (γ control, 47.5 ± 19.2 Hz nA^{-1}; γ post-conditioning, 61.2 ± 25.6 Hz nA^{-1}, $n = 3$ cells; $P \leq 0.01$) and a rightward shift of the *F–I* relation (θ control, 0.05 ± 0.07 nA; θ

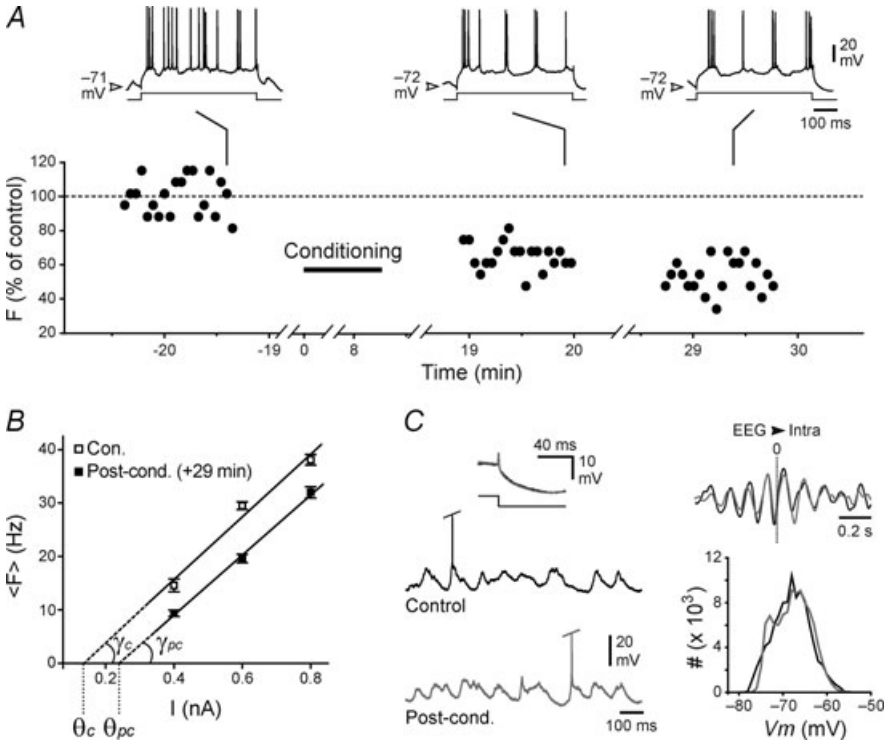

Figure 7. Activity-dependent decrease in cortical neurone intrinsic excitability: rightward shift in the *F–I* curve

A, long-lasting decrease in the firing frequency of a RS cortical neurone, in response to a +0.6 nA current pulse, after application of a conditioning protocol consisting of iterative injection of 101 current pulses of +0.8 nA leading to a mean frequency of 27 Hz. Firing frequencies are normalized to the mean control value (dashed line). Top traces illustrate the firing responses obtained at the indicated times. *B*, *F–I* curves (linear fits, $r^2 > 0.76$; $P < 0.001$) in control (Con.) and 29 min after the conditioning. Each data point is the mean (± S.E.M.) firing rate calculated from 20 successive trials. The value of θ was significantly increased after conditioning (Control, $\theta_c = 0.13$ nA; Post-conditioning, $\theta_{pc} = 0.24$ nA; $P < 0.05$), whereas the corresponding slope of the *F–I* curve was not significantly affected (Control, $\gamma_c = 58.7$ Hz nA^{-1}; Post-conditioning, $\gamma_{pc} = 56.6$ Hz nA^{-1}; $P > 0.5$). *C*, spontaneous intracellular activity (left, bottom traces) and corresponding membrane potential (V_m) (bin, 1 mV) distribution (right, bottom graph) in control (black traces) and after conditioning (grey traces), showing the stability of ongoing synaptic activities and output firing. Consistently, the cross-correlation (with an oscillatory profile at 8.5 Hz) between the EEG and intracellular activities, before (black) and after (grey) conditioning, remained stable (right, top). The constancy of voltage responses (left, top records) to square negative current pulses, before (black traces) and after (grey traces) the induction protocol, demonstrates that the passive membrane properties were not affected. Action potentials in the illustrated intracellular spontaneous activities are truncated for clarity. All results illustrated in this figure are from the same paired recording.

post-conditioning, 0.2 ± 0.01 nA, $n = 3$ cells; $P \leq 0.01$). This was not correlated with modification in passive membrane properties ($P > 0.2$ for each parameter) and the spontaneous firing rate (1.4 ± 0.8 Hz in control, $n = 3$ cells) was unaffected by the conditioning. These mixed changes in intrinsic parameters within the same cell, which have opposite influences on membrane excitability parameters, led, however, to consistent cellular changes, i.e. an increase ($n = 2$ cells) or a decrease ($n = 1$ cell) in the firing in response to the limited range of tested inputs. Nevertheless, it is plausible that such complex plastic processes would have led to differential effects on cell responsiveness for a wider range of stimulus intensities.

Heterogeneous expression of intrinsic plasticity in pyramidal motor cortex neurones

Twenty-one of the 33 conditioned neurones (63.6%) exhibited significant modifications in their membrane excitability (Fig. 9*B*), which were not associated with changes in the passive membrane properties. In the remaining cells ($n = 12$, 11 RS and 1 IB), the induction protocols (53–105 current pulses of 0.3–1.0 nA; evoked firing rate ranged from 11 to 60 Hz) had no significant effect on current threshold, slope of the *F–I* curves (Fig. 9*A*), basic membrane properties or spontaneous firing rate.

As described above, layer V motor cortex pyramidal neurones could exhibit *in vivo* an increase or a decrease of their membrane excitability, which resulted from a selective change in θ, γ (Fig. 9*A*) or a modification in both parameters (Fig. 9*B* and *C*). The graph in Fig. 9*C* depicts the relationship between γ and θ, before (open symbols) and after (filled symbols) induction of plasticity, in each cell that experienced significant changes in intrinsic excitability. This representation illuminates the high cell-to-cell heterogeneity in the degree and direction of modifications in θ and γ.

We searched for a possible relationship between the directionality of the plasticity and the corresponding cellular or conditioning parameters. Conditioned neurones were categorized into three groups: global potentiation, global depression and lack of change in membrane excitability. We then compared the corresponding mean values of control membrane potential, input resistance, spontaneous firing rate, conditioning protocol duration, evoked firing rate during conditioning stimulations and total number of action potentials during the induction protocol. No significant differences were found ($P > 0.05$ for each parameter), indicating that the sign of intrinsic plasticity did not depend upon the conditioning parameters or the passive neuronal electrophysiological properties, at least those that could be measured by our intrasomatic recordings.

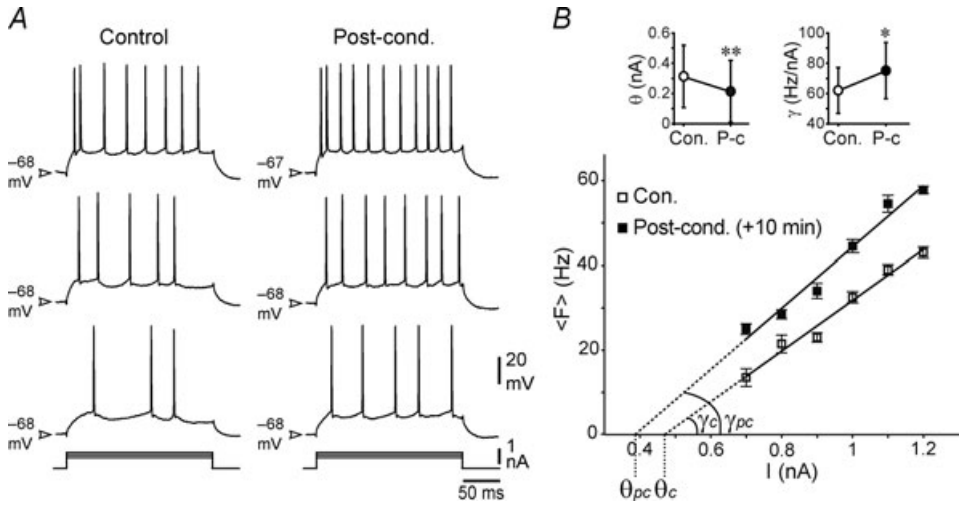

Figure 8. Mixed intrinsic plasticity in a potentiated cortical neurone
A, current (bottom traces)-evoked firing (top traces) in a RS motor cortex neurone, in control and 10 min after conditioning (Post-cond.), which consisted of repetitive application of 80 current pulses of 1.1 nA inducing a mean firing of 36 Hz. Note the increase in evoked firing for all tested current intensities whereas the membrane potential remained stable (arrowheads). *B,* corresponding *F–I* curves (linear fits, $r^2 > 0.8$; $P < 0.001$) in control (Con.) and 10 min after conditioning protocol. The slope was increased by 21% (Control, $\gamma_c = 59.9$ Hz nA^{-1}; +10 min, $\gamma_{pc} = 72.3$ Hz nA^{-1}; $P = 0.02$) with a concomitant decrease of 17% in the current threshold (Control, $\theta = 0.47$ nA; +10 min, $\theta_{pc} = 0.39$ nA; $P = 0.01$). Each data point corresponds to the mean ($\pm$ S.E.M.) response calculated from 10 successive trials. The inset indicates the pooled values of θ (left graph) and γ (right graph), in control (Con.) and after conditioning (P-c), in the 3 neurons exhibiting a mixed 'coherent' intrinsic potentiation (*$P < 0.05$; **$P < 0.01$).

Discussion

The purpose of the present study was to examine the changes in membrane excitability that can occur *in vivo* in pyramidal motor cortex neurones after repeated direct stimulations. Most conditioned neurones exhibited durable intrinsic changes expressed as an increase or a decrease in global cell excitability. Potentiated neurones showed either an enhancement in the slope of the *F–I* relationship, a decrease in the threshold current associated with a leftward shift of the *F–I* curve or concomitant modifications of both parameters. Depressed cells mostly exhibited an augmentation in the current threshold associated with a rightward shift in the *F–I* curve. Experience-dependent intrinsic plasticity was not correlated with modifications in passive membrane properties, pointing out the role of voltage-gated ion channels in its expression.

Induction and expression of intrinsic plasticity in neocortical neurones

Activity-dependent intrinsic plasticity in neocortical pyramidal neurones has already been reported *in vitro* (Desai *et al.* 1999; Sourdet *et al.* 2003; Cudmore & Turrigiano, 2004) and *in vivo* (Woody *et al.* 1991; Aou *et al.* 1992). However, the present study provides, to our knowledge, the first detailed description on the impact of intrinsic plasticity in the input–output function of neocortical cells *in vivo*.

A chronic synaptic deprivation of cultured cortical pyramidal neurones induces a homeostatic intrinsic

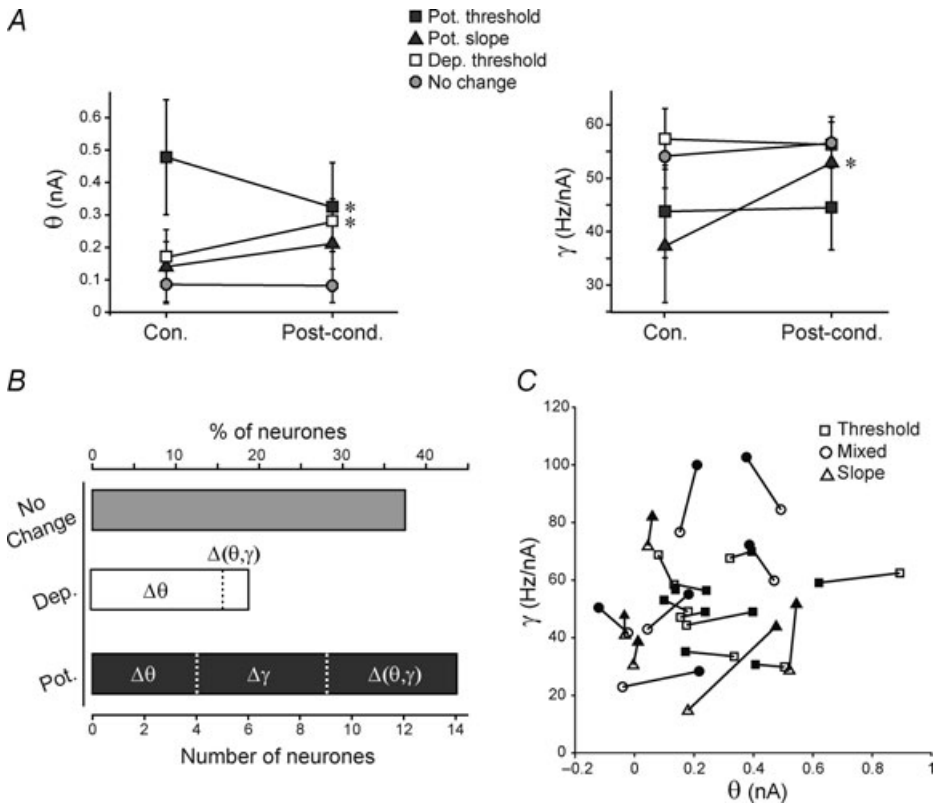

Figure 9. Various forms of intrinsic plasticity in layer V motor cortex pyramidal neurones
A, pooled values of θ (left graph) and γ (right graph), before (Con.) and after (Post-cond.) conditioning, for the different groups of conditioned neurones including, no change in intrinsic excitability (No change, $n = 12$), potentiation of intrinsic excitability due to a decrease in θ (Pot. threshold, $n = 4$), potentiation of intrinsic excitability due to an increase in γ (Pot. slope, $n = 5$) and decrease of intrinsic excitability due to an increase in θ (Dep. threshold, $n = 5$) (*$P < 0.05$). *B,* summarized data indicating the number and the percentage of neurones showing activity-dependent potentiation (Pot.), depression (Dep.) or stability (No change) in their membrane excitability. The relative proportion of neurones displaying a change in the *F–I* slope ($\Delta\gamma$), current threshold ($\Delta\theta$) or in both parameters simultaneously ($\Delta(\gamma,\theta)$) is indicated. *C,* group result showing in individual neurones (connected symbols) the relationship between the change in γ and θ. Neurones were categorized according to the expression of intrinsic plasticity: modification in current threshold (Threshold), modification in both γ and θ (Mixed) and modification in the *F–I* curve slope (Slope). The open and filled symbols correspond to control and post-conditioning conditions, respectively.

plasticity, which is expressed by an increase in the initial slope of the *F–I* curve and a decrease in the threshold current (Desai *et al.* 1999). In visual cortical slices, repeated periods of postsynaptic firing, a conditioning procedure similar to the one we used, result exclusively in a potentiation of intrinsic excitability, expressed as a leftward shift of the entire *F–I* curve without any modification in its slope (Cudmore & Turrigiano, 2004). In sensorimotor cortex neurones *in vitro*, patterned synaptic stimulations induce a decrease in the threshold current together with an increase in the slope of the *F–I* relationship (see Fig. 4*A* in Sourdet *et al.* 2003), leading to a global enhancement of cellular excitability. Interestingly, the *in vivo* activity-dependent intrinsic plasticity we induced in motor cortex neurones using repeated direct stimulations shares some expression properties with that obtained in conscious cats in the same cell type following rapid acquisition of eye blink conditioning (Aou *et al.* 1992). After conditioning, the enhanced unit activity in the cat motor cortex was correlated with a decrease in the intensity of intracellularly applied current required for spike initiation, without affecting the resting membrane potential (Aou *et al.* 1992). However, a systematic analysis of the input–output relationship of the recorded neurones was not performed in this study and possible changes in the *F–I* curves could have been overlooked.

Heterogeneous intrinsic plasticity in a homogeneous population of neurones

The present study demonstrates for the first time that a homogeneous population of neurones, here the layer V pyramidal cells of the motor cortex, can undergo *in vivo* a diversity of activity-dependent intrinsic changes in response to similar conditioning protocols. Activity-dependent modifications of the threshold stimulus or the slope of the *F–I* relationship might result from modifications of distinct ion channels. Pyramidal cortical neurones express a large repertoire of voltage- and calcium-gated ion channels that can be actively regulated, including fast and persistent sodium currents, rapidly inactivating, after-hyperpolarization, and tetraethylammonium-sensitive potassium currents and inwardly cationic rectifying currents (Desai *et al.* 1999; Egorov *et al.* 2002; Sourdet *et al.* 2003; Chen *et al.* 2007; Cohen-Matsliah *et al.* 2007; Yoshida & Alonso, 2007). The fact that a significant proportion of neurones displayed mixed forms of intrinsic plasticity, where both the threshold and the gain were modified, suggests that distinct activity-dependent processes of intrinsic plasticity were simultaneously involved. A similar coordinate participation of different intrinsic mechanisms has been observed in pyramidal cortical neurones during long-lasting intrinsic plasticity (Desai *et al.* 1999).

Moreover, the sign and magnitude of each type of plasticity could result from the specific membrane state of each neurone, i.e. the degree of active ion channel phosphorylation, which reflects the history of cell activity (Marder *et al.* 1996; Daoudal *et al.* 2002; Delord *et al.* 2007). In addition, the variability in excitability changes could arise from *in vivo* neuromodulatory processes, such as cholinergic (Egorov *et al.* 2002) or dopaminergic (Chen *et al.* 2007) systems known to differentially modulate membrane excitability (Steriade, 2004). It is also plausible that continuous interactions between neurone-specific electrical membrane properties and changing ongoing synaptic activities (Paré *et al.* 1998) lead to a cell-to-cell variability in the expression of intrinsic changes.

Putative mechanisms of intrinsic plasticity

The present data, obtained by *in vivo* intracellular recordings, provide little information on the cellular mechanisms underlying the multiple forms of intrinsic plasticity we unveiled in motor cortex neurones. However, it is plausible that the changes in intrinsic excitability, which were expressed by modifications in the current threshold and/or in the slope of *F–I* curves, reflect modulations of different types of voltage-gated ion channels, operating just below or above spike threshold. Moreover, because intrinsic plasticity was induced after periods of repeated firing, it is likely that its induction results from a rise in the intracellular concentration of calcium (Xu & Kang, 2005; Delord *et al.* 2007).

A use-dependent decrease in current threshold, leading to a global increase of cell excitability, has been already reported in various brain regions including hippocampus (Ganguly *et al.* 2000; Daoudal *et al.* 2002; Xu *et al.* 2005), cerebellar cortex (Armano *et al.* 2000), deep cerebellar nuclei (Aizenman & Linden, 2000), striatum (Mahon *et al.* 2003, 2004) and neocortex (Cudmore & Turrigiano, 2004). In visual cortex neurones *in vitro*, an induction protocol similar to that used in our study induces a decrease in the threshold current and voltage resulting from a calcium- and protein kinase A-dependent alteration of conductances available around spike threshold (Cudmore & Turrigiano, 2004). In hippocampal pyramidal neurones, a similar activity-dependent potentiation of intrinsic excitability has been directly attributed to a hyperpolarizing shift in the activation curve of voltage-gated sodium channels (Ganguly *et al.* 2000; Xu *et al.* 2005).

Conversely, the post-conditioning increase in the slope of *F–I* curves might originate from alterations in voltage-gated conductances available at suprathreshold levels. In vestibular nucleus neurones, an enhancement in the gain of the input–output relationship, triggered by brief periods of inhibitory synaptic stimulations, is due to a

down-regulation of calcium-activated potassium channels underlying after-hyperpolarization (Nelson *et al.* 2003). A similar mechanism has been found in sensorimotor cortex neurones *in vitro* (Sourdet *et al.* 2003) and in pyramidal hippocampal cells (Disterhoft *et al.* 1986; Coulter *et al.* 1989) and pyriform cortex neurones (Saar *et al.* 1998) after learning procedures.

These intrinsic mechanisms, increasing the cell excitability at sub- and suprathreshold levels, could be responsible, separately or in conjunction, for the increased excitability we observed in motor cortex *in vivo*. As an example of concomitant changes in both current threshold and slope of the *F–I* curve, bath application of dopamine has been found to induce in motoneurones an alteration in calcium-dependent potassium channels, leading to an increase of the neuronal gain, concomitantly with a decrease in the rheobasic current, which was attributed to an alteration in A-type potassium current (Han *et al.* 2007).

Although there have been few descriptions of activity-dependent decrease in membrane excitability compared to intrinsic potentiation, its expression could account for homeostatic (van Welie *et al.* 2004; Fan *et al.* 2005) or learning-dependent (Daoudal *et al.* 2002; Li *et al.* 2004) processes. In our study, the attenuation of intrinsic excitability, mainly expressed as a rightward shift of the *F–I* curves, could result from a calcium-dependent enhancement of slowly-inactivating potassium currents (Li *et al.* 2004).

A possible role in memory formation

Our data demonstrate that changes in neuronal excitability can be induced in motor cortex neurones *in vivo* by repeated firing patterns resembling those generated in these cells during associative learning (Birt *et al.* 2003). In addition, experience-dependent intrinsic plasticity has been reported in the motor cortex after eye-blink conditioning in the cat (Woody *et al.* 1991; Aou *et al.* 1992). Altogether, these observations suggest that the use-dependent intrinsic plasticity we described could provide a potent cellular mechanism for memory storage. The heterogeneous and bidirectional intrinsic plasticity may profoundly affect the collective behaviour within the conditioned cortical network and participate in the setting of adapted temporal and spatial patterns of neuronal activity. Indeed, the experience-dependent decrease in current threshold could lower the minimal strength of synaptic input required to generate an action potential (Daoudal *et al.* 2002; Sourdet *et al.* 2003; Mahon *et al.* 2004) and thus allow the recruitment of additional neurones that were silent prior to conditioning. On the other hand, the increase in the neuronal gain might enhance the cell responsiveness to suprathreshold synaptic inputs and possibly promote neuronal synchronization. Indeed, the potentiation of membrane excitability of sensorimotor cortex neurones *in vitro* can enhance the temporal fidelity of action potential discharge among conditioned cells (Sourdet *et al.* 2003). An opposite impact on synaptic networks may occur during the depression of intrinsic excitability, which might lower the firing rate of individual cells and/or reduce the pool of active neurones. Finally, combined modifications in the current threshold and the slope of the *F–I* curve could amplify the contrast of responses to weak and strong stimuli. For instance, a concomitant increase in both parameters will enhance the neuronal selectivity and responsiveness to synaptic inputs.

Hence, during a learning task, heterogeneous and bidirectional experience-dependent intrinsic changes, which could act in concert with bidirectional long-term synaptic plasticity (Bear, 1996; Sanes & Donoghue, 2000; Kim & Linden, 2007 for reviews), might shape and lay down the new cortical network activities underlying the learned motor engram.

References

Aizenman CD & Linden DJ (2000). Rapid, synaptically driven increases in the intrinsic excitability of cerebellar deep nuclear neurons. *Nat Neurosci* **3**, 109–111.

Aou S, Woody CD & Birt D (1992). Increases in excitability of neurons of the motor cortex of cats after rapid acquisition of eye blink conditioning. *J Neurosci* **12**, 560–569.

Armano S, Rossi P, Taglietti V & D'Angelo E (2000). Long-term potentiation of intrinsic excitability at the mossy fibre-granule cell synapse of rat cerebellum. *J Neurosci* **20**, 5208–5216.

Baranyi A, Szente MB & Woody CD (1993). Electrophysiological characterization of different types of neurons recorded in vivo in the motor cortex of the cat. II. Membrane parameters, action potentials, current-induced voltage responses and electrotonic structures. *J Neurophysiol* **69**, 1865–1879.

Bear MF (1996). A synaptic basis for memory storage in the cerebral cortex. *Proc Natl Acad Sci U S A* **93**, 13453–13459.

Bear MF (2003). Bidirectional synaptic plasticity: from theory to reality. *Philos Trans R Soc Lond B Biol Sci* **358**, 649–655.

Birt D, Aou S & Woody CD (2003). Intracellularly recorded responses of neurons of the motor cortex of awake cats to presentations of Pavlovian conditioned and unconditioned stimuli. *Brain Res* **969**, 205–216.

Chen L, Bohanick JD, Nishihara M, Seamans JK & Yang CR (2007). Dopamine D1/5 receptor-mediated long-term potentiation of intrinsic excitability in rat prefrontal cortical neurons: Ca^{2+}-dependent intracellular signaling. *J Neurophysiol* **97**, 2448–2464.

Cohen-Matsliah SI, Brosh I, Rosenblum K & Barkai E (2007). A novel role for extracellular signal-regulated kinase in maintaining long-term memory-relevant excitability changes. *J Neurosci* **27**, 12584–12589.

Connors BW & Gutnick MJ (1990). Intrinsic firing patterns of diverse neocortical neurons. *Trends Neurosci* **13**, 99–104.

Coulter DA, Lo Turco JJ, Kubota M, Disterhoft JF, Moore JW & Alkon DL (1989). Classical conditioning reduces amplitude and duration of calcium-dependent afterhyperpolarization in rabbit hippocampal pyramidal cells. *J Neurophysiol* **61**, 971–981.

Creutzfeld OT, Watanabe S & Lux HD (1966). Relations between EEG phenomena and potentials of single cortical cells. II. Spontaneous and convulsoid activity. *Electroenceph Clin Neurophysiol* **20**, 19–37.

Cudmore RH & Turrigiano GG (2004). Long-term potentiation of intrinsic excitability in LV visual cortical neurons. *J Neurophysiol* **92**, 341–348.

Daoudal G & Debanne D (2003). Long-term plasticity of intrinsic excitability: learning rules and mechanisms. *Learn Mem* **10**, 456–465.

Daoudal G, Hanada Y & Debanne D (2002). Bidirectional plasticity of excitatory postsynaptic potential (EPSP)-spike coupling in CA1 hippocampal pyramidal neurons. *Proc Natl Acad Sci U S A* **99**, 14512–14517.

Delord B, Berry H, Guigon E & Genet S (2007). A new principle for information storage in an enzymatic pathway model. *PLoS Comput Biol* **3**, e124.

Desai NS, Rutherford LC & Turrigiano GG (1999). Plasticity in the intrinsic excitability of cortical pyramidal neurons. *Nat Neurosci* **2**, 515–520.

Disterhoft JF, Coulter DA & Alkon DL (1986). Conditioning-specific membrane changes of rabbit hippocampal neurons measured *in vitro*. *Proc Natl Acad Sci U S A* **83**, 2733–2737.

Egorov AV, Hamam BN, Fransén E, Hasselmo ME & Alonso AA (2002). Graded persistent activity in entorhinal cortex neurons. *Nature* **420**, 173–178.

Fan Y, Fricker D, Brager DH, Chen X, Lu HC, Chitwood RA & Johnston D (2005). Activity-dependent decrease of excitability in rat hippocampal neurons through increases in I_h. *Nat Neurosci* **8**, 1542–1551.

Feldman MD (1984). Morphology of the neocortical pyramidal neuron. In *Cerebral Cortex*, ed. Peters A & Jones EG, pp. 123–200. Plenum Press, New York.

Ganguly K, Kiss L & Poo M-M (2000). Enhancement of presynaptic neuronal excitability by correlated presynaptic and postsynaptic spiking. *Nat Neurosci* **3**, 1018–1026.

Golowasch J, Casey M, Abbott LF & Marder E (1999). Network stability from activity-dependent regulation of neuronal conductances. *Neural Comput* **11**, 1079–1096.

Han P, Nakanishi ST, Tran MA & Whelan PJ (2007). Dopaminergic modulation of spinal neuronal excitability. *J Neurosci* **27**, 13192–13204.

Kim SJ & Linden DJ (2007). Ubiquitous plasticity and memory storage. *Neuron* **56**, 582–592.

Li CY, Lu JT, Wu CP, Duan SM & Poo MM (2004). Bidirectional modification of presynaptic neuronal excitability accompanying spike timing-dependent synaptic plasticity. *Neuron* **41**, 257–268.

Mahon S, Casassus G, Mulle C & Charpier S (2003). Spike-dependent intrinsic plasticity increases firing probability in rat striatal neurons *in vivo*. *J Physiol* **550**, 947–959.

Mahon S, Deniau JM & Charpier S (2001). Relationship between EEG potentials and intracellular activity of striatal and cortico-striatal neurons: an *in vivo* study under different anaesthetics. *Cereb Cortex* **11**, 360–373.

Mahon S, Deniau JM & Charpier S (2004). Corticostriatal plasticity: life after the depression. *Trends Neurosci* **27**, 460–467.

Marder E (1998). From biophysics to models of network function. *Annu Rev Neurosci* **21**, 25–45.

Marder E, Abbott LF, Turrigiano GG, Liu Z & Golowasch J (1996). Memory from the dynamics of intrinsic membrane currents. *Proc Natl Acad Sci U S A* **93**, 13481–13486.

Martin SJ & Morris RG (2002). New life in an old idea: the synaptic plasticity and memory hypothesis revisited. *Hippocampus* **2**, 609–636.

Nelson AB, Krispel CM, Sekirnjak C & du Lac S (2003). Long-lasting increases in intrinsic excitability triggered by inhibition. *Neuron* **40**, 609–620.

Paré D, Shink E, Gaudreau H, Destexhe A & Lang EJ (1998). Impact of spontaneous synaptic activity on the resting properties of cat neocortical pyramidal neurons in vivo. *J Neurophysiol* **79**, 1450–1460.

Paxinos G & Watson C (1986). *The Rat Brain in Stereotaxic Coordinates*. Academic Press, Sydney.

Paz JT, Deniau JM & Charpier S (2005). Rhythmic bursting in the cortico-subthalamo-pallidal network during spontaneous genetically determined spike and wave discharges. *J Neurosci* **25**, 2092–2101.

Polack P-O & Charpier S (2006). Intracellular activity of cortical and thalamic neurons during high-voltage rhythmic spike discharge in Long-Evans rats *in vivo*. *J Physiol* **571**, 461–476.

Rall W (1969). Time constants and electrotonic length of membrane cylinders and neurons. *Biophys J* **9**, 1483–1508.

Saar D, Grossman Y & Barkai E (1998). Reduced after-hyperpolarization in rat piriform cortex pyramidal neurons is associated with increased learning capability during operant conditioning. *Eur J Neurosci* **10**, 1518–1523.

Sanes JN & Donoghue JP (2000). Plasticity and primary motor cortex. *Annu Rev Neurosci* **23**, 393–415.

Sokal RR & Rohlf FJ (1995). *Biometry: The Principles and Practice of Statistics in Biological Research*. WH Freeman and Company, New York.

Sourdet V, Russier M, Daoudal G, Ankri N & Debanne D (2003). Long-term enhancement of neuronal excitability and temporal fidelity mediated by metabotropic glutamate receptor subtype 5. *J Neurosci* **23**, 10238–10248.

Steriade M (2004). Neocortical cell classes are flexible entities. *Nat Rev Neurosci* **5**, 121–134.

van Welie I, van Hooft JA & Wadman WJ (2004). Homeostatic scaling of neuronal excitability by synaptic modulation of somatic hyperpolarization-activated I_h channels. *Proc Natl Acad Sci U S A* **101**, 5123–5128.

Woody CD, Gruen E & Birt D (1991). Changes in membrane currents during Pavlovian conditioning of single cortical neurons. *Brain Res* **539**, 76–84.

Xu J & Kang J (2005). The mechanisms and functions of activity-dependent long-term potentiation of intrinsic excitability. *Rev Neurosci* **16**, 311–323.

Xu J, Kang N, Jiang L, Nedergaard M & Kang J (2005). Activity-dependent long-term potentiation of intrinsic excitability in hippocampal CA1 pyramidal neurons. *J Neurosci* **25**, 1750–1760.

Yoshida M & Alonso A (2007). Cell-type specific modulation of intrinsic firing properties and subthreshold membrane oscillations by the M(Kv7)-current in neurons of the entorhinal cortex. *J Neurophysiol* **98**, 2779–2794.

Zhang W & Linden DJ (2003). The other side of the engram: experience-driven changes in neuronal intrinsic excitability. *Nat Rev Neurosci* **4**, 885–900.

Author contributions

S.C., B.D. and S.M. conceived the conceptual framework of the study and designed the experiments. J.T.P., S.C., S.M. and P.T. performed the experiments. J.T.P., S.M., P.T., S.G., B.D. and S.C. participated in the analysis and the interpretation of the data. S.C., S.M. and B.D. wrote the manuscript and J.T.P., P.T. and S.G. revised and improved it. All the authors have approved the final version of the manuscript.

Acknowledgements

This work was supported by grants from the Action Concertée Incitative (ACI 'Temps et Cerveau'), the Institut National de la Santé et de la Recherche Médicale and the Université Pierre et Marie Curie (Paris 6). We thank Pierre-Olivier Polack for valuable comments on an early version of the manuscript, Anne-Marie Godeheu for histological expertise, Morgane Pidoux and Jean-Michel Deniau for constructive discussions.